Technometrics

ISSN: 0040-1706 (Print) 1537-2723 (Online) Journal homepage: https://www.tandfonline.com/loi/utch20

Constrained Varying-Coefficient Model for Time-Course Experiments in Soft Tissue Fabrication

Qian Wu, Xinwei Deng, Shiren Wang & Li Zeng

To cite this article: Qian Wu, Xinwei Deng, Shiren Wang & Li Zeng (2020): Constrained Varying-Coefficient Model for Time-Course Experiments in Soft Tissue Fabrication, Technometrics, DOI: 10.1080/00401706.2020.1731604

To link to this article: https://doi.org/10.1080/00401706.2020.1731604

TECHNOMETRICS
2020, VOL. 00, NO. 0, 1–14
https://doi.org/10.1080/00401706.2020.1731604

Taylor & Francis
Taylor & Francis Group

Constrained Varying-Coefficient Model for Time-Course Experiments in Soft Tissue Fabrication

Qian Wu[a], Xinwei Deng[b], Shiren Wang[a], and Li Zeng[a]

[a]Department of Industrial and Systems Engineering, Texas A&M University, College Station, TX; [b]Department of Statistics, Virginia Tech, Blacksburg, VA

ABSTRACT

In the fabrication of artificial soft tissues, novel biomaterials with the required properties are obtained by appropriately adjusting process parameters during material synthesis. One key step in finding the desired material is understanding the relationship between the process parameters and the material properties, and time-course experiments are typically conducted for this purpose. This article proposes a constrained varying-coefficient modeling method for such data in which expert knowledge is properly accommodated in the model estimation to make the modeling practically meaningful. The proposed model has a semiparametric structure and incorporates expert knowledge in the form of constraints on model coefficients. Estimation algorithms based on a smoothing spline and a weighted smoothing spline are also provided. Finally, the proposed method is compared with existing methods in a case study and a numerical study.

ARTICLE HISTORY
Received September 2018
Accepted February 2020

KEYWORDS
Biomaterial fabrication;
Constrained modeling;
Time-course experiment;
Varying-coefficient model;
Weighted smoothing spline

1. Introduction

Soft tissue injury occurs frequently among the elderly, due to the combination of long-term pressure and the decline of physiological functions. Consequently, there is a substantial and increasing demand for soft tissue repair and replacement surgeries (World Health Organization 2011; Ortman, Velkoff, and Hogan 2014; Parker et al. 2016). Among various treatments for soft tissue injury, soft tissue grafts are one of the favored treatments for the long term. However, there is a large gap between the demand for and the supply of soft tissue grafts due to a shortage of donations (Weiss et al. 2017). Driven by the need to close this gap, fabrication of artificial (engineered) soft tissues has become an emerging research topic.

A key to the success of soft tissue fabrication lies in appropriate biomaterials. For given biomaterial types, the use of 3D printing allows the fabrication of structures with complicated and customized shapes, such as human tissue for each individual patient (He, Xue, and Fu 2015). Figure 1 illustrates the concept of 3D printing for fabricating soft tissue products, using the meniscus as an example. It begins with acquiring an image of the tissue by a medical scanner such as computed tomography (CT) or magnetic resonance imaging (MRI). Then the image is processed to create a computer-aided design (CAD) model, and the tissue is printed layer by layer based on the CAD model (Wei et al. 2015).

To serve the proper functions of natural tissues, the fabricated products need to meet certain requirements. Again, take an artificial meniscus as an example. It must have certain mechanical properties when exposed to shear, tension, and compression forces (Bochynska et al. 2016), since the meniscus acts as a cushion for the knee joint to maintain its stability. Moreover, the meniscus is lubricated, so it is necessary to consider the surface characteristics of the product (Fox, Bedi, and Rodeo 2012). In addition, the biocompatibility of the product is crucial, as it will be implanted in a human body.

In biomaterial fabrication, satisfactory material properties depend on the settings of the process parameters (e.g., percentages of ingredients, heating temperature). It is important to understand the relationship between the process parameters and material properties, or the effect of the process parameters on material properties. Data-driven methods are useful for modeling such effects, since the fabrication involves a series of physicochemical mechanisms that are complex or unknown. This requires data about the material properties that result from different settings of the process parameters. Also, as the effect of the process parameters evolves with time, the dynamic trajectory of the material properties needs to be measured to characterize the stability of the tissue products, which is critical for serving their designed functions. Such data are obtained by conducting time-course experiments as illustrated in the upper panel of Figure 2, where y is the material property and x is the process parameter of interest. Within the cost budget, m different settings of the process parameter, $x_1, \ldots, x_m$, are considered. Under the ith setting, the material is fabricated and values of y at n time points, denoted as $y_i\left(t_j\right), i = 1, \ldots, m, j = 1, \ldots, n$, are measured. The collected data form a two-way table, as shown in the lower panel of Figure 2. Graphically, they manifest as multiple time-course curves, each for a setting of the process parameter.

Several considerations are involved in modeling the data in Figure 2. First, because the modeling is intended to provide a

CONTACT Li Zeng lizeng@tamu.edu Department of Industrial and Systems Engineering, Texas A&M University, College Station, TX 77843.
Supplementary materials for this article are available online. Please go to www.tandfonline.com/r/TECH.

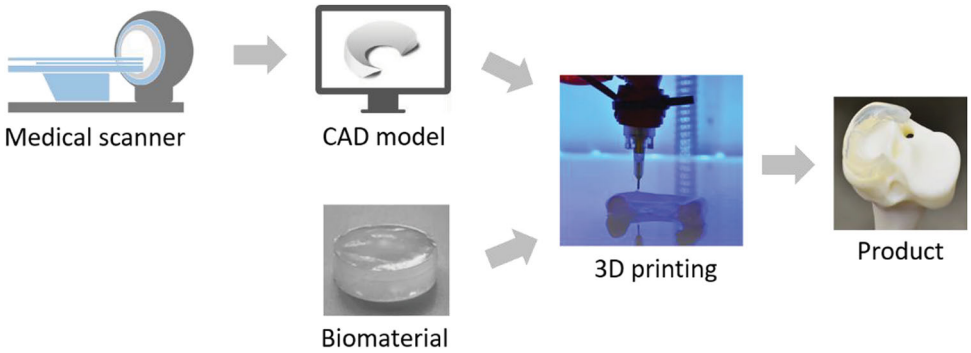

Figure 1. An illustration of 3D printing for fabricating an artificial meniscus.

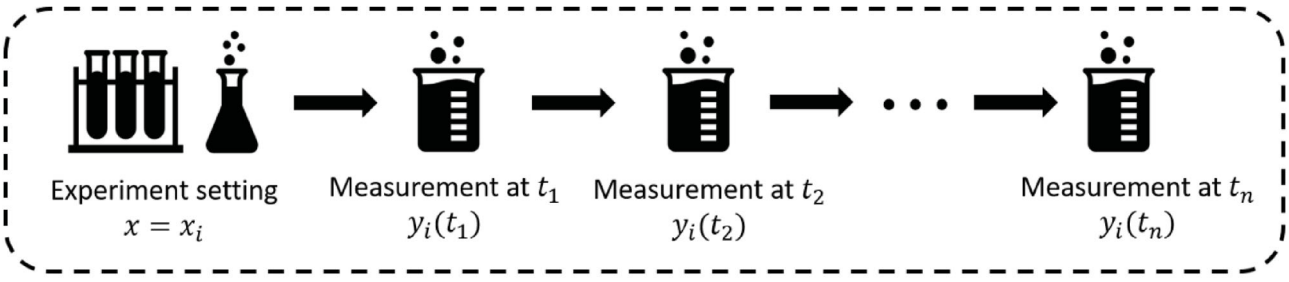

Setting	t_1	t_2	...	t_n
x_1	$y_1(t_1)$	$y_1(t_2)$	...	$y_1(t_n)$
⋮	⋮	⋮	...	⋮
x_m	$y_m(t_1)$	$y_m(t_2)$	...	$y_m(t_n)$

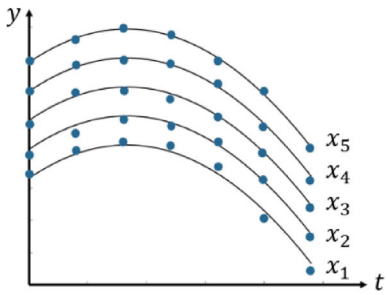

Figure 2. Data collected in biomaterial experiments, where $y_i(t_j)$ is the measurement of the material property for the process parameter value x_i and time t_j.

better understanding of the complex material fabrication process, good interpretability is required. Second, expert or domain knowledge about the process must be accommodated to make the estimated model practically meaningful. Finally, the model must be applicable to a small amount of data, as experiments in the fabrication of soft tissues are costly and time-consuming.

For the preceding reasons, we adopt a modeling strategy based on varying-coefficient models (VCMs) (Hastie and Tibshirani 1993). The key idea in conventional VCMs is to use a linear (or nonlinear) function to model the relationship between the response and the covariates, where the coefficients (including the intercept) are nonparametric functions of time. Thus, they can capture both the complex effects of the covariates and the dynamics of the effects. With a linear form, these models are also easy to understand and do not require large samples for fitting. However, one limitation of conventional VCMs is that they are not easy to accommodate expert knowledge.

In this work, we propose a constrained VCM method to model such time-course data as illustrated in Figure 2, with accommodation of expert knowledge in the biomaterial fabrication. The proposed model is a linear function of covariates with *semiparametric* coefficients. The intercept is a parametric function of time, and the coefficient of the covariate is a nonparametric function of time. Such a semiparametric model structure allows expert knowledge to be accommodated in the form of constraints on the model coefficients. Specifically, knowledge about the baseline material property is incorporated by specifying an appropriate form for the parametric intercept function, while knowledge about the effect of the process parameter on the material property is incorporated by imposing constraints on the nonparametric coefficient function. For the latter, we consider a dynamic stability constraint that applies in many engineering applications. We also develop model estimation methods based on a smoothing spline and a weighted smoothing spline for the proposed model.

This work makes three contributions. First, it establishes an interpretable framework for modeling data from time-course experiments in soft tissue fabrication. The proposed methodology can be applied to broader areas, such as biomanufacturing, with similar forms of experimental data. It can obtain a model with good interpretability to help researchers learn new knowledge about their processes. Second, we develop novel ways to accommodate different types of engineering expert knowledge on data analytics for better interpretation and prediction. Finally, the use of a weighted smoothing spline in the proposed method provides a new and convenient way to impose constraints in nonparametric function estimation. Smoothing splines are known to be sensitive to large random errors/outliers

in real observations. By imposing constraints through a weighting scheme, we can regulate the smoothing spline fitting and make it satisfy various requirements for specific applications.

The remainder of this article is organized as follows. Section 2 reviews the related literature. Section 3 describes the proposed modeling method and explains the underlying idea. Section 4 presents the model estimation algorithms. Section 5 applies the proposed method to a dataset from artificial meniscus fabrication and compares its interpretability and prediction performance with those of existing methods. Section 6 provides a numerical example to illustrate the advantage of accommodating expert knowledge in statistical modeling. Section 7 concludes this study and discusses future work.

2. Literature Review

The form of the time-course data in Figure 2 is similar to the longitudinal/panel data that are popular in economics, social sciences, and medical literature (Islam 1995; Hsiao 2003). There are three relevant modeling approaches in the literature. (1) *Marginal or population-averaged models* assume that the response (the biomaterial property in our problem) is a linear model of covariates (the process parameters for biomaterial fabrication) through some link function (Verbeke et al. 2008). Some studies use a nonparametric intercept to improve model flexibility (Zeger and Diggle 1994). The effects of covariates on the response are represented by their coefficients, but the dynamics of the effects are often not captured. Moreover, an adequate link function may not be available in practice to characterize the complex effects of covariates. (2) *Mixed-effect models* use a linear function to model the relationship of the response and covariates with random effects for quantifying the randomness between samples (Laird and Ware 1982). They are often used for panel data from individuals, such as patients in a medical study, where between-individual variation is of interest. However, this is not the case in this study. (3) *Transition models* account for the time dependence of the response using Markov models (Verbeke et al. 2008). The effect of a covariate is separated into two parts, as represented by its coefficient in the regression component of the model and by the influence of past values of the response on its present value. Such an approach is not applicable for our problem since biomaterial fabrication requires a direct characterization of the effect of the process parameters.

Imposing constraints in statistical modeling has recently been studied. For example, the recently developed shape-constrained generalized additive model (SCAM) can incorporate shape constraints such as monotonicity (Pya and Wood 2015). A constrained hierarchical model has been proposed for modeling the degradation of biomaterials, with monotonicity and concavity constraints incorporated in the model (Zeng, Deng, and Yang 2016). Several studies have developed constrained Gaussian process modeling, in which shape and other types of constraints such as bound and censoring are considered (Lin and Dunson 2014; Wang and Berger 2016; Lenk and Choi 2017; Zeng, Deng, and Yang 2018). Splines with a nonnegativity constraint have been used for analyzing the wake effect in wind turbine power generation (Hwangbo, Johnson, and Ding 2018). The present work considers a *dynamic stability constraint* on the effect of process parameters that has not yet been considered in the literature.

3. The Proposed Model

Let y be the measurement of the biomaterial property of interest (e.g., toughness or viscosity), x the value of a process parameter (e.g., the percentage of a certain ingredient or temperature) in biomaterial fabrication, and t the time. We consider the VCM

$$y(t) = \beta_0(t) + \beta_1(t)\, x + \epsilon(t), \quad \epsilon(t) \sim N\left(0, \sigma_\epsilon^2\right), \qquad (1)$$

where $\beta_0(t;\theta)$ is a parametric function with parameter θ and $\beta_1(t)$ is a nonparametric function.

Here $\epsilon(t)$ is a Gaussian white noise process that represents the overall effect of measurement errors and other random errors in the fabrication. The error term is assumed to be normally distributed with mean 0 and a constant variance σ_ϵ^2. $\beta_0(t)$ is the intercept, and $\beta_1(t)$ is the coefficient of the process parameter.

The proposed model in Equation (1) follows the spirit of conventional VCMs, which allow the coefficients to evolve with time to capture the dynamics of the effect of a process parameter. It has a linear structure with respect to the process parameter, and thus a large number of different settings of the process parameter are not required for learning the model. This is especially useful for the application we consider, where only a limited number of settings are affordable in experimental studies. The linear structure is also easy to interpret. These aspects of the model make it suitable for the data in Figure 2.

The core of the proposed model lies in the coefficients $\beta_0(t)$ and $\beta_1(t)$, which need good interpretations and provide a foundation for accommodating expert knowledge. Specifically, the intercept term $\beta_0(t)$ represents the material property under the null setting of the process parameter (i.e., $x = 0$), or the baseline material property. We consider a *parametric* function of time for $\beta_0(t)$ since the baseline material property is often relatively straightforward with abundant domain knowledge (Murphy, Black, and Hastings 2016), including physiochemical models of the material and historical data on the material characterization. The slope term $\beta_1(t)$ represents the effect of the process parameter on the material property. In general, this effect is complex, and there is little available knowledge about it, especially in new fabricated biomaterials. Therefore, we assume that $\beta_1(t)$ is a *nonparametric* function of time.

The above setup makes it convenient to incorporate different types of expert knowledge in the form of constraints on the two coefficients. Specifically, expert knowledge about the baseline material property can be incorporated by constraining the form of $\beta_0(t)$ (e.g., specifying a certain parametric form for $\beta_0(t)$), and knowledge about the effect of the process parameter can be incorporated by imposing constraints on the nonparametric fitting of $\beta_1(t)$. Examples of such constraints are sign constraints (e.g., the effect must be positive) and shape constraints (e.g., the effect must be monotonically nondecreasing over time).

The idea of expert knowledge accommodation is illustrated in Figure 3 with a simple example. The observed data are shown in the left panel of the figure, and the coefficients and fitted values are shown in the right panel. Assume that we have the

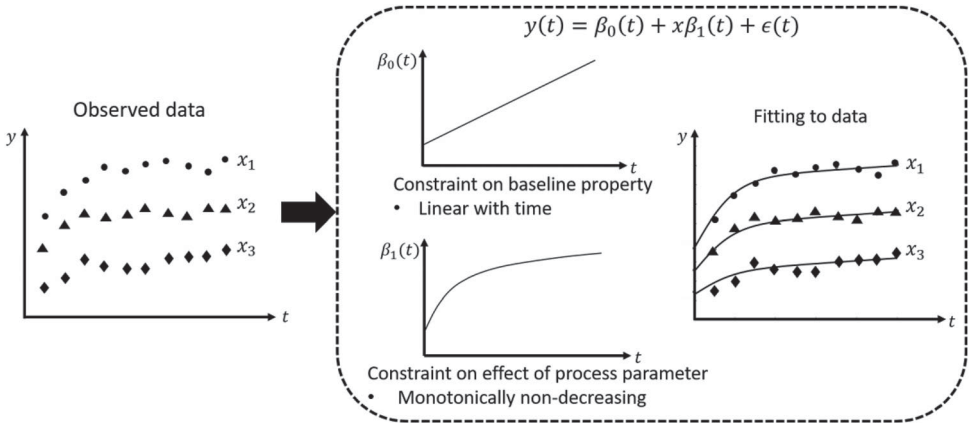

Figure 3. The idea of expert knowledge accommodation in the proposed modeling method.

following expert knowledge: under the baseline setting, the material property approximately linearly increases over time, and the effect of the process parameter is monotonically non-decreasing over time. Accordingly, $\beta_0(t)$ is modeled as a linear function of time, while $\beta_1(t)$ is a nonparametric function of time with a monotonicity constraint. The modeling is expected to produce a good fit to the observed data and estimates of the two coefficients that reveal the baseline material property and the effect of the process parameter on the material property, as shown in the right panel of Figure 3.

4. Model Estimation

Suppose that the time-course data contain m settings of the process parameter, $x_1, x_2, \ldots, x_m$, and measurements of the material property at n time points for each setting. Using i to index the process settings and j to index the time points, the matrix form of the proposed model can be written as

$$\boldsymbol{Y}\left(t_j\right) = \beta_0\left(t_j\right)\mathbf{1}_{m\times 1} + \beta_1\left(t_j\right)\boldsymbol{X} + \boldsymbol{\epsilon}\left(t_j\right), \quad j = 1, \ldots, n, \quad (2)$$

where $\boldsymbol{Y}(t_j) = (y_1\left(t_j\right), \ldots, y_m(t_j))'$, $\mathbf{1}_{m\times 1} = (1, \ldots, 1)'$, $\boldsymbol{X} = (x_1, \ldots, x_m)'$, and $\boldsymbol{\epsilon}\left(t_j\right) = (\epsilon_1\left(t_j\right), \ldots, \epsilon_m(t_j))'$.

For the model estimation, we consider the following two scenarios.

Scenario 1. There is only expert knowledge about the baseline material property. In this scenario, the parametric form of $\beta_0(t;\theta)$ is determined by the expert knowledge about the baseline material property, and $\beta_1(t)$ takes a general nonparametric form. A method to estimate the parameter θ of $\beta_0(t)$ and $\beta_1(t)$ is described in Section 4.1.

Scenario 2. There is expert knowledge about both the baseline material property and the effect of the process parameter. In this scenario, in addition to the parametric form of $\beta_0(t;\theta)$ determined by the expert knowledge about the baseline material property, some constraints are imposed on the nonparametric form of $\beta_1(t)$ to reflect the expert knowledge about the effect of the process parameter on the material property. In particular, we will investigate a dynamic stability constraint that is a characteristic feature of biomaterials and also a common phenomenon in many engineering applications. Section 4.2 describes how this constraint is imposed in the estimation of $\beta_1(t)$.

4.1. Estimation Under Scenario 1

In this scenario, we consider a smoothing spline as the nonparametric function for $\beta_1(t)$, since the process parameter usually has a continuous smooth effect over time. Thus, the model estimation can be written as

$$\begin{aligned}&\left(\widehat{\theta}^*, \widehat{\beta}_1^*(t)\right)\\ &= \underset{\theta,\beta_1(t)}{\arg\min} \sum_{i=1}^{m}\sum_{j=1}^{n}\left\{\left[y_i\left(t_j\right) - \beta_0\left(t_j;\theta\right) - x_i\beta_1\left(t_j\right)\right]^2\right\}\\ &\quad + \lambda\int \beta_1''(t)\,dt, \end{aligned} \quad (3)$$

where λ is a smoothing parameter. As there are two unknowns—the parametric component θ (and $\beta_0(t;\theta)$) and the nonparametric component $\beta_1(t)$—the estimation will follow an iterative scheme in a similar fashion to the generalized semiparametric VCMs (Qi, Sun, and Gilbert 2017). To differentiate it from the constrained estimate of $\beta_1(t)$ in Scenario 2, we will refer to $\widehat{\beta}_1^*(t)$ as the unconstrained estimate of $\beta_1(t)$.

Figure 4 depicts the idea of the iterative estimation procedure. The estimation has two building blocks: the estimation of $\beta_1(t)$ by the smoothing spline and the estimation of θ by the parametric function fitting. The estimation begins by assigning an initial value to θ. Given the value of θ (and thus $\beta_0(t;\theta)$), an estimate of $\beta_1(t)$ is obtained by fitting the adjusted part, $\{\boldsymbol{Y}\left(t_j\right) - \beta_0\left(t_j;\widehat{\theta}\right)\boldsymbol{I}_{m\times 1}, j = 1, \ldots, n\}$, using the smoothing spline. Similarly, given the estimate of $\beta_1(t)$, an estimate of θ is obtained by fitting the function $\beta_0(t;\theta)$ to the adjusted part, $\{\boldsymbol{Y}\left(t_j\right) - \boldsymbol{X}\widehat{\beta}_1\left(t_j\right), j = 1, \ldots, n\}$. This process iterates to update the estimates of θ and $\beta_1(t)$ until $\widehat{\theta}$ converges. The steps of this method are summarized in Algorithm 1 of Appendix A in the supplementary materials.

More specifically, in the estimation of $\beta_1(t)$ given $\widehat{\theta}$, the smoothing spline method for conventional VCMs is used (Eubank et al. 2004). This method gives an analytical solution for

$$\begin{aligned}\widehat{\beta}_1(t) &= \underset{\beta_1(t)}{\arg\min} \sum_{i=1}^{m}\sum_{j=1}^{n}\left\{\left[\widetilde{y}_i\left(t_j\right) - x_i\beta_1\left(t_j\right)\right]^2\right\}\\ &\quad + \lambda\int \beta_1''(t)\,dt, \end{aligned} \quad (4)$$

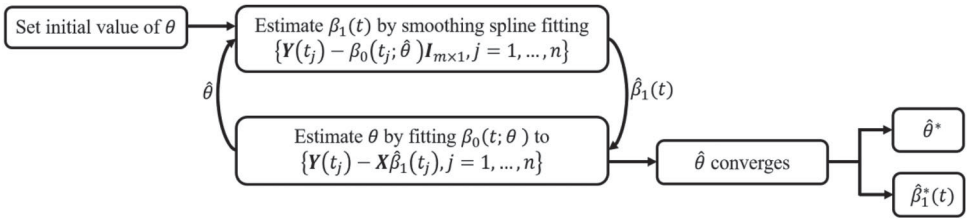

Figure 4. An illustration of the model estimation under Scenario 1.

where $\widetilde{y}_i(t_j) = y_i(t_j) - \beta_0(t_j;\widehat{\theta})$. The objective function in Equation (4) contains two parts: the residual sum of squares (RSS), which represents the goodness of fit, and the penalty for non-smoothness, which is controlled by the smoothing parameter λ. A number of methods for automatic smoothing parameter selection are available in the literature, including prediction-based methods such as cross-validation (Wahba and Wold 1975), generalized cross-validation (GCV) (Craven and Wahba, 1978), Mallow's C_p (Wakefield 2013), and the improved Akaike information criterion (Hurvich, Simonoff, and Tsai 1998); likelihood-based methods such as maximum likelihood (Anderssen and Bloomfield 1974), generalized maximum likelihood (Wahba 1985), and restricted maximum likelihood (Wood 2011); and risk-based methods (Lee 2003). In our study, we use GCV for the smoothing parameter selection, as it is widely used in the VCMs literature (e.g., Eubank et al. 2004).

The estimation of θ given $\widehat{\beta}_1(t)$ is a nonlinear (linear if $\beta_0(t;\theta)$ is linear) least-squares curve fitting problem

$$\widehat{\theta} = \arg\min_{\theta} \sum_{i=1}^{m}\sum_{j=1}^{n} \left(r_i(t_j) - \beta_0(t_j;\theta)\right)^2, \tag{5}$$

where $r_i(t_j) = y_i(t_j) - x_i\widehat{\beta}_1(t_j)$. Optimization problem (5) can be solved by either the trust-region-reflective algorithm (Moré 1978) or the Levenberg–Marquardt algorithm (Coleman and Li 1996).

4.2. Estimation Under Scenario 2

Dynamic stability means that the material property approaches an equilibrium state as time passes. In biomaterial fabrication, it is common expert knowledge that the material property under each setting of the process parameter will stabilize over time, which implies that the effect of the process parameter $\beta_1(t)$ will converge to a constant. Note that the data-driven approach may not follow such an underlying mechanism, since it relies on data to reveal the pattern of the observed data. The smoothing spline method used in Section 4.1 could thus fit the experimental data well, but might not produce a $\widehat{\beta}_1(t)$ with the desired shape, especially when the data suffer from large random errors and/or outliers, which often happens in biomaterial experiments.

To address this challenge, we consider a constrained smoothing spline for the estimation of $\beta_1(t)$ that incorporates dynamic stability as a constraint, as follows:

$$\widehat{\beta}_1(t) = \begin{cases} \arg\min_{\beta_1(t)} \sum_{i=1}^{m}\sum_{j=1}^{n} \left\{\left[y_i(t_j) - \beta_0(t_j;\widehat{\theta}^*) - x_i\beta_1(t_j)\right]^2\right\} \\ \qquad +\lambda \int \beta_1''(t)\,dt \\ \qquad \text{s.t. } \beta_1(t) \text{ converges as } t \to \infty \end{cases}, \tag{6}$$

where $\widehat{\theta}^*$ is the estimate of θ obtained from the unconstrained scenario in Section 4.1. Here θ is treated as a known plug-in parameter, considering that in general, the parametric function (i.e., $\beta_0(t;\theta)$) fitting is not as flexible as the nonparametric fitting. If θ is treated as an unknown under the constrained scenario, it can be difficult to find an estimate of θ that both fits $\beta_0(t;\theta)$ adequately and satisfies the constraint. Thus, it is better to obtain the estimate of θ under the simpler unconstrained scenario and then apply the flexible nonparametric fitting of $\beta_1(t)$ to the adjusted data, $y_i(t) - \beta_0(t;\widehat{\theta}^*)$.

Note that the formulation in Equation (6) is not easy to solve, because the constraint is rather implicit and nonlinear. It might be thought that the dynamic stability constraint can be integrated in the objective function in a penalty form similar to the non-smoothness penalty. However, the non-smoothness penalty is a global constraint that applies for the entire time span of $\beta_1(t)$, while the dynamic instability penalty is local and only used in the tail part of the function. It would be complex to implement this penalty, including defining the tail of $\beta_1(t)$ and solving the resultant optimization problem for parameter estimation.

To circumvent this difficulty, we consider a weighted smoothing spline method and adjust the weights appropriately so that the estimate $\widehat{\beta}_1(t)$ converges over time. The reasoning here is to allow more bias at some points through the weighting scheme, forcing the resultant estimate to satisfy the constraint. Specifically, we use the following weighted smoothing spline to obtain $\widehat{\beta}_1(t)$:

$$\widehat{\beta}_1(t) = \arg\min_{\beta_1(t)} \sum_{i=1}^{m}\sum_{j=1}^{n} w_{ij}\left\{\left[y_i(t_j) - \beta_0(t_j;\widehat{\theta}^*) - x_i\beta_1(t_j)\right]^2\right\} + \lambda\int \beta_1''(t)dt, \tag{7}$$

where w_{ij} is the weight given to the squared error under the ith setting at time t_j, $i = 1,\ldots,m, j = 1,\ldots,n$. If all the weights are equal to 1, the weighted smoothing spline reduces to a smoothing spline, and if a weight w_{ij} is less than 1, more bias is allowed in fitting the corresponding data point. The closed-form solution of Equation (7) and details of the derivation can be found in Appendix B in the supplementary materials.

It should be mentioned that the weighted smoothing spline in the literature is usually used for improving the local performance of curve fitting. That is, weights are assigned to either the squared error term or the smoothness penalty term in Equation (4) to reduce bias in a region with large local variation (Maria and Malva 2005; Davies and Meise 2008). Our use of the weighted smoothing spline in the present work has an opposite purpose: allowing tolerable bias in the fitting when local vari-

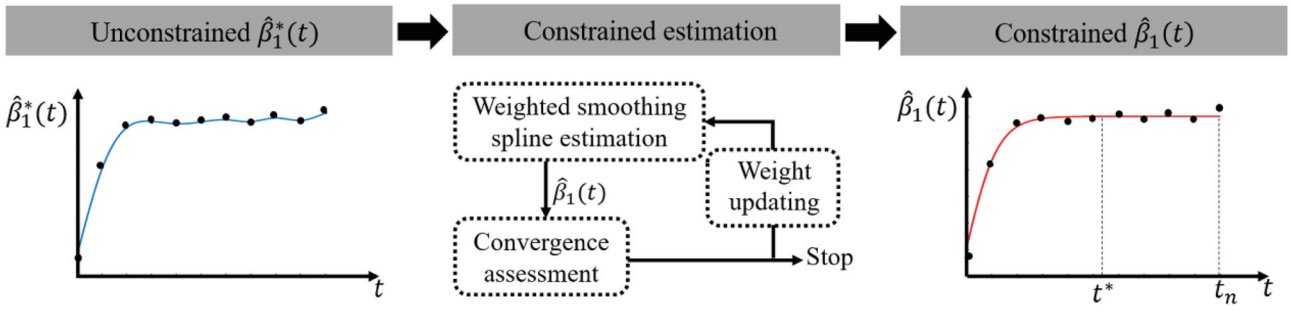

Figure 5. The proposed method to incorporate the dynamic stability constraint in the estimation of $\beta_1(t)$.

ation is large to make the estimate $\widehat{\beta}_1(t)$ satisfy the dynamic stability constraint.

Based on the weighted smoothing spline in Equation (7), a satisfactory estimate of $\beta_1(t)$ for the constrained estimation problem in Equation (6) is found through an iterative search. The idea is illustrated in Figure 5. Basically, the constrained estimate of $\beta_1(t)$ in the right panel is obtained by correcting the unconstrained estimate $\widehat{\beta}_1^*(t)$ in the left panel so that the resulting estimate exhibits converging behavior during the period $[t^*, t_n]$ (later called the converging stage), where t^*, $0 < t^* \leq t_n$, is the starting time point. Specifically, starting with $\widehat{\beta}_1^*(t)$, we update the weights w_{ij} in Equation (7) and iteratively obtain a new estimate $\widehat{\beta}_1(t)$ from the weighted smoothing spline. The convergence performance of the estimate from each iteration is assessed. This will produce a number of estimates for $\beta_1(t)$ and their corresponding convergence assessments before the stopping condition is met, and the one that has the best convergence performance will be selected as the constrained estimate of $\beta_1(t)$. The steps of this method are summarized in Algorithm 2 of Appendix C in the supplementary materials.

We use $C_{\widehat{\beta}_1} = \int_{t^*}^{t_n} |\widehat{\beta}_1'(t)| dt$ to assess the convergence performance of the estimate $\widehat{\beta}_1(t)$. Obviously, a smaller value of $C_{\widehat{\beta}_1}$ indicates better convergence performance for $\widehat{\beta}_1(t)$. As shown in Appendix B of the supplementary materials, $\widehat{\beta}_1(t)$ is a natural cubic spline, and thus $\widehat{\beta}_1'(t)$ can be computed using the natural cubic basis functions and their estimated coefficients.

The weight updating is to improve the convergence performance of $\widehat{\beta}_1(t)$. Here we propose an updating method based on the current fitting performance:

$$w_{ij} = \frac{\min_{1 \leq i' \leq m, a \leq j' \leq n} |r_{i'j'}|}{|r_{ij}|}, \quad i = 1, \ldots, m, j = a, \ldots, n, \tag{8}$$

where $r_{ij} = y_i(t_j) - \widehat{y}_i(t_j)$ is the residual of the current fitting, a is the time index corresponding to the starting time t^* of the converging stage, and $w_{ij} = 1$ for $j < a$. The idea here is similar to that of robust regression (Rousseeuw 1987). If there exist any observations with large random errors or outliers, those points are given small weights. Thus, large bias is allowed in fitting them—or, in other words, they will have little influence on the estimation. Since those points are, as mentioned previously, the major cause for non-convergence, this is expected to improve the convergence performance of $\widehat{\beta}_1(t)$.

Implementing the estimation method proposed in Figure 5 requires solving three other related issues. First, the dynamic stability constraint should be imposed on the converging stage $[t^*, t_n]$ in the constrained estimation. There is usually no knowledge about the starting time t^* of the converging stage, and it needs to be automatically estimated from the data. Second, in addition to good converging behavior, the constrained estimation should also ensure acceptable fitting accuracy. Note that the weights in the weighted smoothing spline vary from iteration to iteration, which means that the fitting accuracy can also vary, and the resultant estimate may not have satisfactory accuracy. We check the fitting accuracy in each iteration and end the search when it becomes unacceptable. Finally, appropriate values should be selected for the tuning parameters. Details of how to solve these issues are presented next.

4.2.1. Estimating the Starting Time t* of the Converging Stage

The reverse cumulative average, that is, the cumulative average starting from the last time point, is often used to reveal the trend of a time-course data stream (Yang, Bitetti-Putzer, and Karplus 2004). Following this idea, for a single time-course stream from the i th setting, $i = 1, \ldots, m$, we can calculate the difference between $y_i(t_j)$, $j = 1, \ldots, n$, and its corresponding reverse cumulative average, denoted as $D_j(i)$. The converging stage of this single stream can then be obtained by finding the time point at which $D_j(i)$ starts to become small. For multiple streams under the m settings, we can take the median of all $D_j(i)$, $i = 1, \ldots, m$, denoted as D_j. To determine the magnitude of the D_j that signals converging, we can compare it to $h\widehat{\sigma}$, where h is a prespecified positive value (e.g., 1) and $\widehat{\sigma}$ is the estimated standard deviation of the data.

Formally, the procedure to find the estimate of t^* consists of the following steps.

Step 1. At each time point t_j, calculate the differences between the observations and their corresponding reverse cumulative averages and compute median:

$$D_j = \underset{i}{\text{median}} \left\{ \frac{1}{n-j+1} \sum_{s=j}^{n} y_i(t_s) - y_i(t_j) : i = 1, \ldots, m \right\}, \quad j = 1, \ldots, n.$$

Step 2. Estimate the variance σ^2 of the data:

$$\widehat{\sigma} = \underset{i}{\text{median}} \{\widehat{\sigma}_i : i = 1, \ldots, m\},$$

where $\widehat{\sigma}_i = \frac{1.48}{\sqrt{2}} \text{median} \{|y_i(t_j) - y_i(t_{j-1})| : j = 2, \ldots, n\}$ is the robust variance estimate for the data under each setting (Davies and Meise 2008).

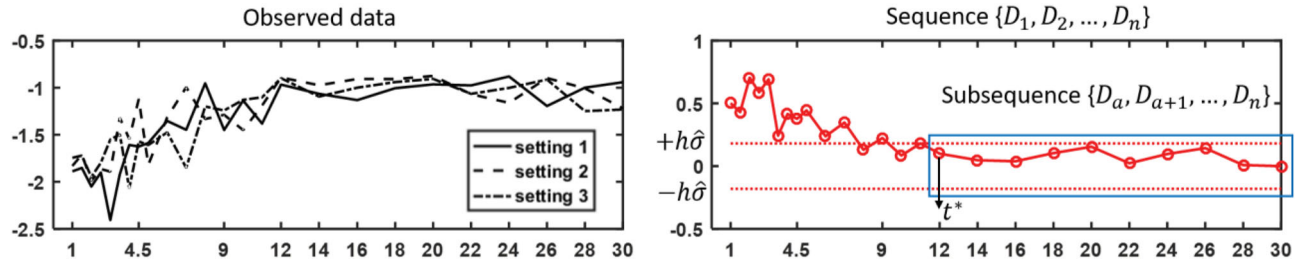

Figure 6. An example of finding the starting time point for the converging stage.

Step 3. In the sequence $\{D_1, D_2, \ldots, D_n\}$, find the longest subsequence $\{D_a, D_{a+1}, \ldots, D_n\}, a \in \{1, \ldots, n\}$, that is bounded by $\pm h\widehat{\sigma}$. Then t_a is the estimate of t^*.

Figure 6 provides an example with $m = 3$ settings and $n = 25$ time points to illustrate the above procedure. Intuitively, when convergence behavior is present, the D_j's are small, as shown in the right panel. $h\widehat{\sigma}$ is used as the threshold to decide whether the sequence is small enough to signal converging. The width of the signaling region depends on the value of h; a larger value of h tolerates more random errors. In the example given in Figure 6, $h = 1$ is used. The 16th time point is selected as the estimate of t^*, and thus the converging stage is $[t_{16}, t_n]$.

4.2.2. Ensuring Acceptable Fitting Accuracy

In some studies (e.g., Davies and Meise 2008), fitting accuracy is controlled by specifying a nonparametric confidence region based on residuals, and the fitting lying in the region is selected. Inspired by this idea, we can guarantee fitting accuracy by defining a region of acceptable accuracy (RAA) for the fitted values $\widehat{y}_i\left(t_j\right) = \beta_0\left(t;\widehat{\theta}^*\right) + x_i\widehat{\beta}_1\left(t_j\right), i = 1, \ldots, m, j = 1, \ldots, n$. The width of the RAA depends on one's tolerance of fitting accuracy. Intuitively, if the width $\to \infty$, fitting accuracy is completely ignored in the constrained estimation, while the narrower the width, the higher the accuracy requirement. A reasonable choice of the RAA is the confidence interval based on the observed data

$$A_\alpha = y_i(t_j) \pm t_{1-\frac{\alpha}{2},n-1} \times \frac{\widehat{\sigma}}{\sqrt{n}}, \tag{9}$$

where α is a tuning parameter to control the width of A_α and $\widehat{\sigma}$ is the estimated standard deviation of the data obtained in Step 2 of the procedure in Section 4.2.1. The tuning parameter α follows the rule for selecting the significance level for confidence intervals; some common values are 0.001, 0.01, and 0.05.

A_α will be used for the stopping condition in the search for the constrained estimate of $\beta_1(t)$. Specifically, the iteration process will stop when the number of fitted values falling outside A_α increases. As the search starts with the unconstrained estimate $\widehat{\beta}_1^*(t)$, this means that the fitting accuracy of the constrained estimate should not be considerably worse than the fitting when the convergence constraint is not considered. It should be pointed out that the RAA can also be viewed as a quantification of uncertainty in the constrained estimation, because it gives a bound for the resulting fitted values.

4.2.3. Selecting Tuning Parameters

The proposed constrained estimation involves two tuning parameters: λ in Equation (7), which controls the smoothness level of $\widehat{\beta}_1(t)$, and α in Equation (9), which controls the width of the acceptable accuracy region. For λ, the non-smoothness penalty is a global constraint that should be established before the local dynamic stability constraint is imposed. Thus, the optimal value of λ obtained by GCV in Section 4.1 will be used in the constrained scenario to maintain the same level of smoothness as in the unconstrained scenario. A smaller value of α corresponds to a tighter region of acceptable accuracy, which requires a larger number of iterations in the estimation. We use a moderate value $\alpha = 0.01$ in the case study to avoid too long a searching time while achieving a reasonably good level of fitting accuracy.

5. Case Study

In this section, we apply the proposed method described in Sections 3 and 4 to a real dataset for 3D printing of menisci. The dataset comes from the fabrication of a novel biomaterial called calcium-alginate/polyacrylamide (CA/PAAm) double-network (DN) hydrogel (Wang et al. 2015). Hydrogel is a popular class of materials constructed by a network of polymer chains. The CA/PAAm-DN hydrogel contains two networks: the alginate/polyacrylamide (A/PAAm) network and the network formed by calcium. With this special structure, the CA/PAAm-DN hydrogel has good shape fidelity with mechanical properties similar to those of a natural meniscus and is hence a promising material for 3D printing of menisci. One key step in synthesizing this type of hydrogel is to immerse the single-network A/PAAm hydrogel in a $CaCl_2$ solution to build the second network through Ca^{2+} in the solution. The concentration of the $CaCl_2$ solution is a critical process parameter in this step that determines the properties of the resulting hydrogel. One property of interest is *swelling*, that is, a change in the volume of the hydrogel, which is important for the geometric fidelity of the 3D printed meniscus. Thus, experiments are conducted to explore how the concentration of the $CaCl_2$ solution affects the swelling behavior of the hydrogel.

Details of the case study are reported in the following subsections. Section 5.1 introduces the data used in the case study and the preprocessing. Section 5.2 describes the available expert knowledge about the baseline swelling behavior of the hydrogel material and the effect of the process parameter on the swelling. Section 5.3 presents the results of the model estimation using the proposed method without and with considering the expert knowledge about the effect of the process parameter. Section 5.4 compares the fitting and prediction performance of the proposed method to those of several existing methods. The data used and the R code can be found in the supplementary materials.

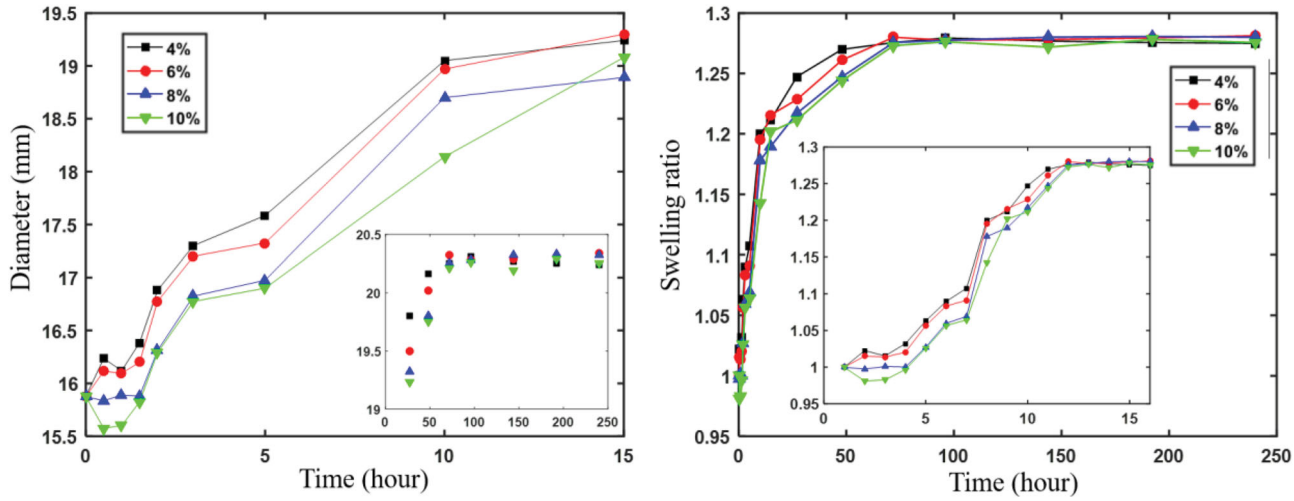

Figure 7. Hydrogel swelling data used in the case study: original (left) and scaled (right).

5.1. Data and Preprocessing

The CA/PAAm-DN hydrogel is made into cylinder-shaped samples under four values of the weight concentration of the $CaCl_2$ solution: 4%, 6%, 8%, and 10%. The diameters of the samples are recorded initially and then measured at 16 time points during a 10-day period. The original data collected from the experiment are displayed in the left panel of Figure 7, with the portions after two days shown in the small plot. We scaled these data by the initial diameter to eliminate the unit effect, so the response used in the modeling is the volumetric swelling ratio rather than the absolute measure of the diameter. The transformed data are displayed in the right panel of Figure 7, where the small plot shows a more detailed view of the data arranged by the time index (i.e., 1st time point, …, 16th time point). We will fit the transformed data using the proposed model in Equation (1). Here y is the volumetric swelling ratio of the fabricated material, x is the weight concentration of the $CaCl_2$ solution, $m = 4$, and $n = 16$.

5.2. Available Expert Knowledge

In the proposed model, the intercept $\beta_0(t)$ represents the swelling behavior of the material when the concentration of the $CaCl_2$ solution is 0% (i.e., when deionized water is used in the material fabrication). In this case, the resulting material is a regular type, single-network hydrogel. $\beta_1(t)$ represents the effect of the concentration of the $CaCl_2$ solution on the swelling behavior of the material. Expert knowledge about these two quantities exists and is described below.

Regarding the swelling behavior of regular hydrogels (i.e., the baseline swelling behavior of the fabricated material), previous research has found that the volume swelling ratio is proportional to the mass swelling ratio, and the mass swelling ratio has a typical behavior pattern that is monotonically nondecreasing and gradually flattens out as time passes (Ehrenhofer, Elstner, and Wallmersperger 2018). In some of the literature, exponential functions are used to fit the mass swelling ratio of various types of hydrogels (Sadeghi and Hosseinzadeh 2013; Slaughter et al. 2015). Thus, we assume that $\beta_0(t)$ has the parametric form:

$$\beta_0(t;\boldsymbol{\theta}) = \theta_1(1 - \theta_2 \cdot e^{-\theta_3 t}), \tag{10}$$

which is characterized by the three parameters $\boldsymbol{\theta} = [\theta_1, \theta_2, \theta_3]$. The parameters have good physical interpretations: θ_1 represents the plateau of the equilibrium volume swelling ratio (i.e., the converged value of the volume swelling ratio), and θ_2 and θ_3 together indicate the rate of increase of the volume swelling ratio before equilibrium is reached (Steiner et al. 2016).

Because the CA/PAAm-DN hydrogel is a new material under development, there exists little understanding in the literature regarding the effect of the $CaCl_2$ concentration on hydrogel swelling. Based on the experimental data in the right panel of Figure 8, a rough impression is that higher concentration leads to a smaller swelling ratio. In other words, the concentration seems to have a negative effect on the swelling. But domain knowledge to support this is lacking. The dynamics of the effect are also unknown; it may monotonically increase or decrease with time or oscillate in a complex way. Hence, we cannot constrain the sign/shape of $\beta_1(t)$, and it needs to be learned from the data. The only knowledge we have is that $\beta_1(t)$ will converge with time. As can be seen from the trend of the data, the swelling of each hydrogel sample will finally reach a plateau, and thus the effect of the process parameter will converge to a constant.

5.3. Model Estimation

We first obtain the estimate of $\beta_0(t)$ using the method described in Section 4.1 (Algorithm 1) and then the estimate of $\beta_1(t)$ with the dynamic stability constraint using the method described in Section 4.2 (Algorithm 2). The parameter setting in the estimation and the results are presented below.

5.3.1. Estimation of $\beta_0(t)$

The initial values of the parameters are set to be $\boldsymbol{\theta}^{(0)} = [\theta_1^{(0)}, \theta_2^{(0)}, \theta_3^{(0)}] = [1, 0.5, 1]$. The algorithm stops after 11 iterations and yields $\widehat{\boldsymbol{\theta}} = [1.28, 0.21, 0.12]$. Figure 8 shows the updating process of the parameter estimation (the 1-norm of $\widehat{\boldsymbol{\theta}}^{(k)} - \widehat{\boldsymbol{\theta}}^{(k-1)}$, where k is the iteration index, is plotted for convenience) and the resulting estimate of $\beta_0(t)$. As expected

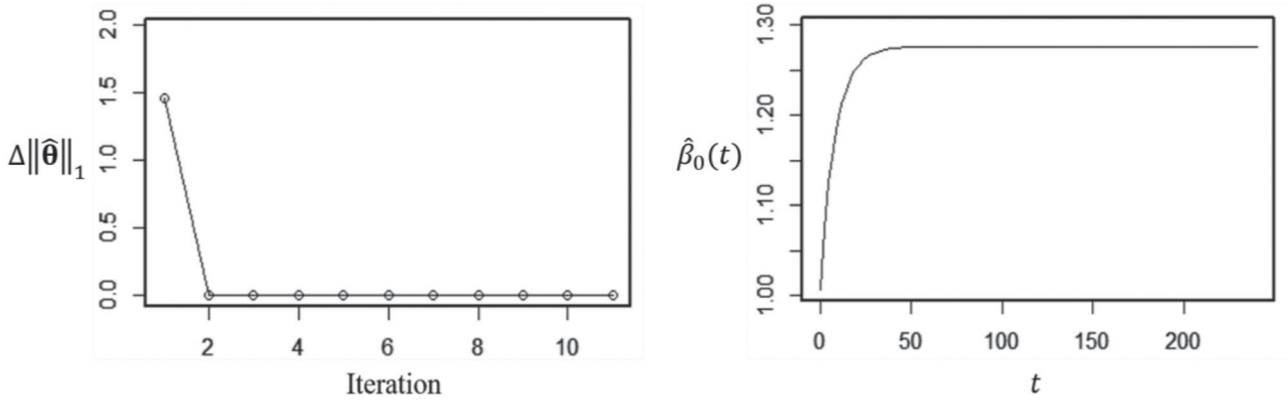

Figure 8. Estimation of $\beta_0(t)$: updating (left) and the resulting estimate of $\beta_0(t)$ (right).

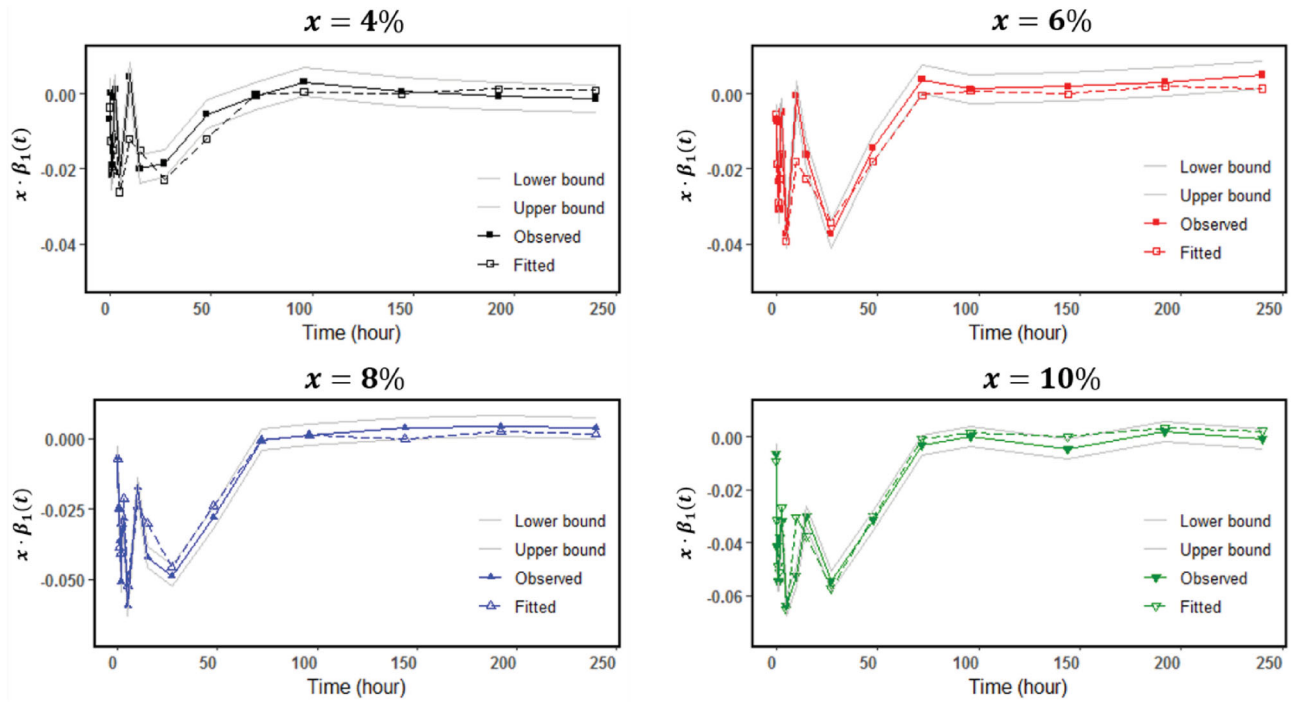

Figure 9. Regions of acceptable accuracy under the four settings of the process parameter.

based on the aforementioned expert knowledge, the estimated $\beta_0(t)$ is nondecreasing and flattens out after approximately 40 hr.

5.3.2. Estimation of $\beta_1(t)$

From the results of Algorithm 1, we have the initial (unconstrained) estimate $\widehat{\beta}_1^{(0)}(t) = \widehat{\beta}_1^*(t)$. To impose the dynamic stability constraint, we first determine the starting point t^* of the converging stage using the procedure given in Section 4.2.1. The standard deviation of the data is estimated to be $\widehat{\sigma} = 0.0137$, and $h = 1$ is used. The starting point is found to be $t^* = t_{12} =$ 72 hr. Then we obtain the region of acceptable accuracy using Equation (9), with $\alpha = 0.01$. The regions associated with the four settings of the process parameter are shown in Figure 9. In each plot, the solid marks connected by solid lines represent the observed values, the hollow marks connected by dash lines represent the fitted values, and the gray lines are the upper and lower bounds of the RAA.

Using Algorithm 2, we obtain the constrained $\widehat{\beta}_1(t)$ with $C_{\widehat{\beta}_1} = 0.0574$, which has a higher degree of convergence than the unconstrained estimate $\widehat{\beta}_1^*(t)$ with $C_{\widehat{\beta}_1^*} = 0.1184$. The two estimates are shown in the left panel of Figure 10, for comparison. It is clear that the constrained estimate is more stable in the tail part. Compared to $\widehat{\beta}_0(t)$ shown in the right panel of Figure 8, the estimated $\beta_1(t)$ has a complex shape during the period $t = [0, 50]$, indicating that the effect of the $CaCl_2$ concentration oscillates in the early stage. This is understandable, because the hydrogel swelling is known to be affected by multiple forces (e.g., shrinkable elastic energy, swelling osmotic energy) that compete before a balance is reached (Wang et al. 2015). Another important finding is that the effect of the $CaCl_2$ concentration is negative, that is, a higher $CaCl_2$concentration tends to shrink the volume of the hydrogel. These findings are useful to researchers studying 3D printing of menisci for understanding the swelling behavior of the novel CA/PAAm-DN hydrogel.

Based on the estimate of $\beta_0(t)$ in Figure 8 and the constrained estimate of $\beta_1(t)$ in the left panel of Figure 10, we obtain the fitted values of the original data on the volume swelling ratio; these are displayed in the right panel of Figure 10. The model

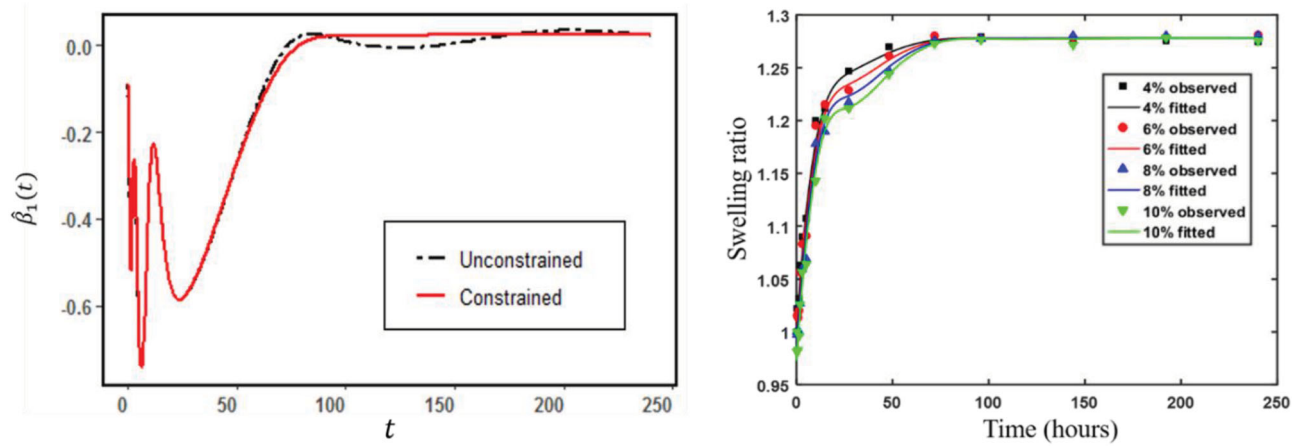

Figure 10. Estimate of $\beta_1(t)$ with and without the dynamic stability constraint (left) and fitted values to the original data (right).

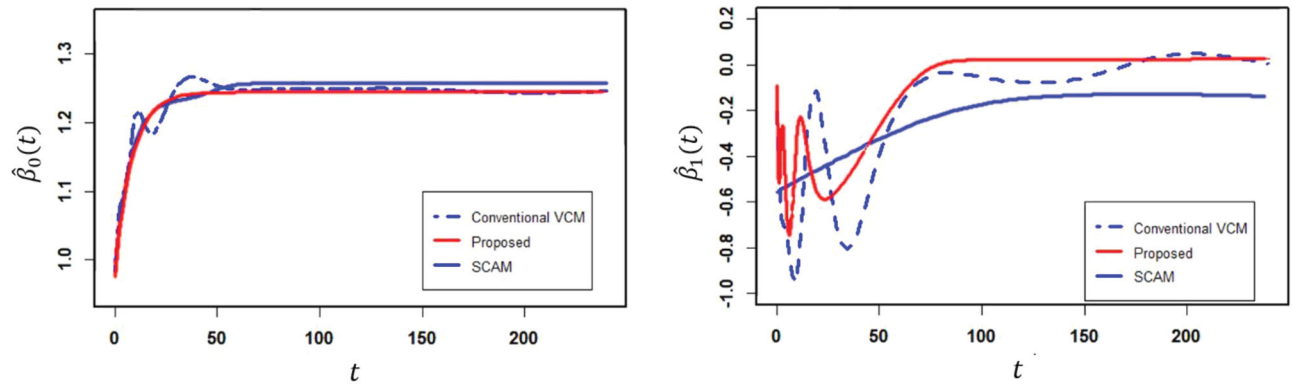

Figure 11. Estimates of $\beta_0(t)$ and $\beta_1(t)$ from conventional VCM, the proposed model, and SCAM with monotonic $\beta_0(t)$.

fitting of the data reaches a sum of squared residuals of 0.0032. The largest fitting error occurs at the point $x = 6, t = 27$ hr, and is only 1.5% of the actual measurement. The residuals (not shown here) are randomly around zero and appear similar for the four settings of the process parameter, which validates the constant variance assumption regarding random errors in Equation (1).

5.4. Comparison With Existing Methods

We compare the proposed model with two existing VCMs: the conventional VCM and the SCAM mentioned in Section 2. For these two methods, both $\beta_0(t)$ and $\beta_1(t)$ are nonparametric functions, except that SCAM can impose shape constraints. They are fitted using the *scam* package in R. The estimated $\beta_0(t)$ and $\beta_1(t)$ of the three methods are given in Figure 11. For the conventional VCM, it can be seen that the nonparametric estimate of $\beta_0(t)$ is jagged, with several local peaks before $t =$ 60 hr, and the estimate of $\beta_1(t)$ has humps in the later stage. Compared to their counterparts in the proposed model, the estimates for the conventional VCM are difficult to interpret and not consistent with expert knowledge.

For the SCAM, we impose a monotonicity constraint on $\beta_0(t)$, since it is known that $\beta_0(t)$ is nondecreasing over time based on expert knowledge about the baseline swelling property of hydrogels. In the results for the SCAM, the estimate of $\beta_0(t)$ has a simple, interpretable shape similar to that of the proposed model, meaning that the monotonicity constraint on $\beta_0(t)$ is helpful. On the other hand, the estimate of $\beta_1(t)$ is over-simplistic. Although the dynamic stability in the later stage is satisfactory, the oscillation in the early stage is completely masked, which is neither consistent with the expert knowledge nor informative in terms of revealing the subtle details of the swelling behavior.

We also compare the prediction performance of the three models. Due to the limited available data, we assess their prediction performance by leave-one-out cross-validation (LOOCV). Specifically, the data at the *jth* time point, $j = 1, \ldots, n$, are used as the test data (of size m), and the remaining data are used as the training data (of size $m \times (n-1)$). We first fit the model using the training data and then predict the responses in the test data. The prediction performance at each data point is measured by the relative prediction error, that is, $\frac{|y_i(t_j) - \widehat{y}_i(t_j)|}{y_i(t_j)}$.

Figure 12 shows the prediction performance of the proposed model and the SCAM (the conventional VCM has similar results, so it is omitted here). Generally speaking, the prediction errors of both models are small (within 4%), indicating good prediction accuracy. Thus, the proposed model has a prediction performance comparable to the two existing VCMs with both $\beta_0(t)$ and $\beta_1(t)$ being nonparametric. Although the original motivation for the proposed model was to enhance model interpretability (by accommodating expert knowledge), it can be seen in Figure 12 that the proposed model also performs well

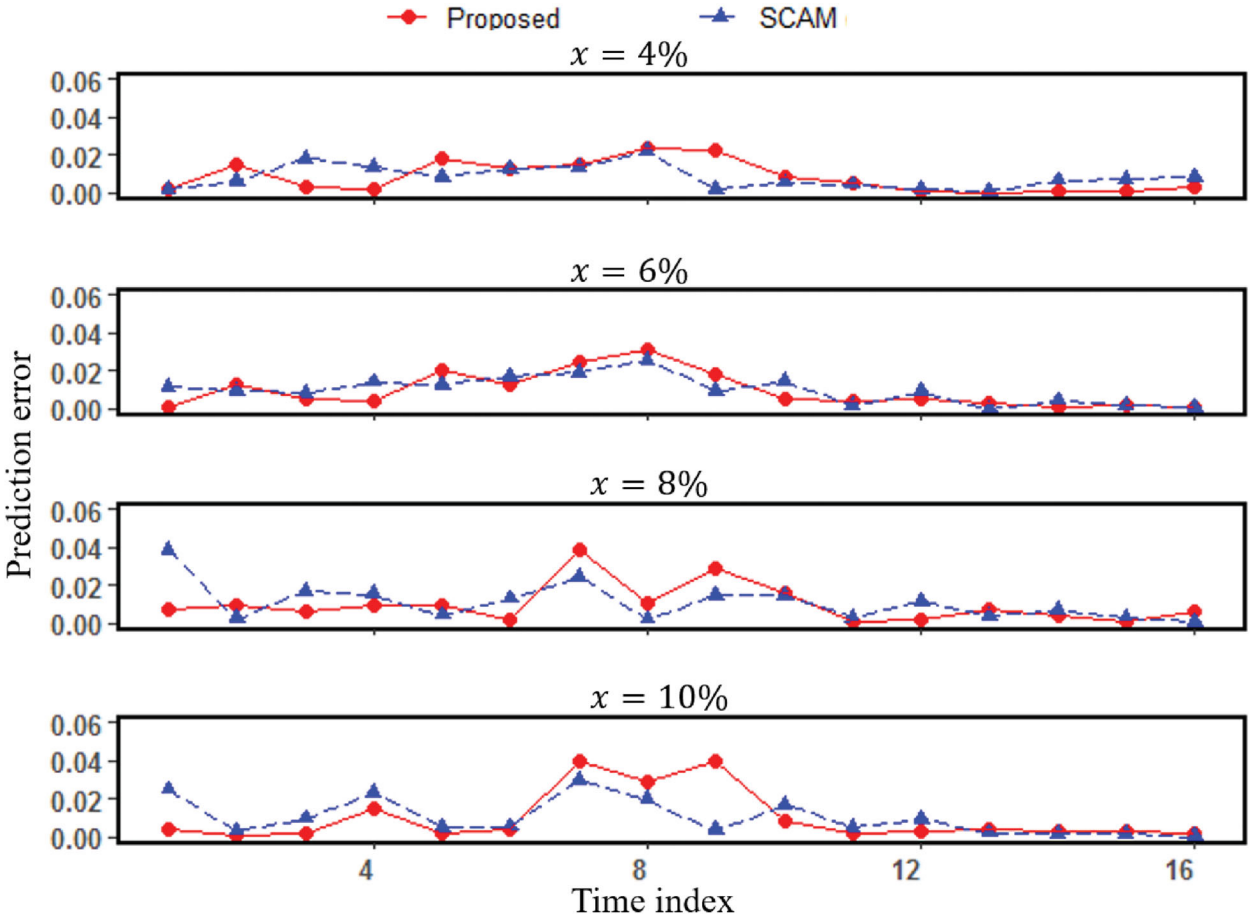

Figure 12. Prediction performance of the proposed model and the SCAM.

in prediction and is comparable to the more flexible VCMs in this respect.

Note that the proposed model performs consistently better in prediction than the SCAM in the later stage, from t_{10} to t_{16}, thanks to the dynamic stability constraint. In addition, the predictions at t_1 are actually extrapolations, as they are made based on data at $t_2, \ldots, t_{16}$. The proposed model has better performance in this case as well, which can be explained by its full accommodation of available expert knowledge about the baseline swelling property and the effect of the process parameter.

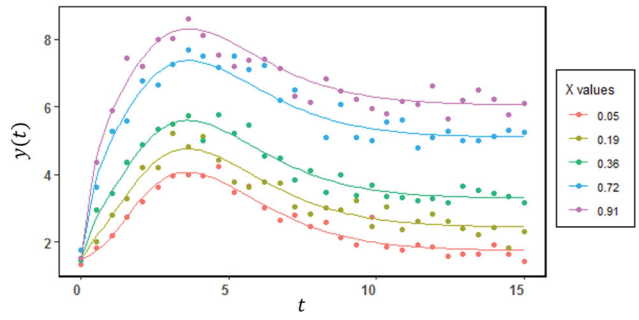

Figure 13. The simulated dataset with $\sigma_\epsilon = 0.3, n = 30$.

6. Numerical Study

To further demonstrate the effectiveness of the proposed method, this section presents a numerical example. The data generation model is

$$\begin{aligned} \boldsymbol{Y}\left(t_j\right) &= \beta_0\left(t_j\right) + \beta_1\left(t_j\right)\boldsymbol{X} + \epsilon\left(t_j\right), \beta_0(t) \\ &= t^{\theta_1} e^{\frac{-t}{\theta_2}} + \theta_3, \beta_1(t) = \frac{\phi_1 t}{\sqrt{\phi_2 + t^2}}, \end{aligned}$$

where the parameters for $\beta_0(t)$ are $\theta_1 = 3$, $\theta_2 = 1.2$, and $\theta_3 = 1.5$, the parameters for $\beta_1(t)$ are $\phi_1 = 5$ and $\phi_2 = 0.4$, $\boldsymbol{X} = [x_1, \ldots, x_m]' = [0.05, 0.19, 0.36, 0.72, 0.91]'$, $\boldsymbol{\epsilon} = \left[\epsilon_1(t_j), \ldots, \epsilon_m(t_j)\right]'$ with $\epsilon_i(t_j) \sim N\left(0, \sigma_\epsilon^2\right)$, and $m = 5$ with n observations for each setting of x. To show the sensitivity of the results to the quality of the data, we consider three different levels of noise variance, $\sigma_\epsilon = 0.3, 0.35, 0.4$, and sample size, $n = 30, 25, 20$.

The simulated data with the best quality, that is, $\sigma_\epsilon = 0.3$, $n = 30$, are shown in Figure 13. In the figure, the curves are the true functions of y for each setting of x (i.e., $\beta_0(t) + \beta_1(t)x_i$, $i = 1, \ldots, m$), and the dots are actual observations. The curves converge when t gets large, whereas the observations do not reflect this trend very well due to considerable random errors. Such a situation is common in biomaterial experiments. We fit the data using the conventional VCM and the proposed model with the dynamic stability constraint. There is no obvious shape requirement in this case, so we do not consider the SCAM. The computation time using the proposed model averages 4 min,

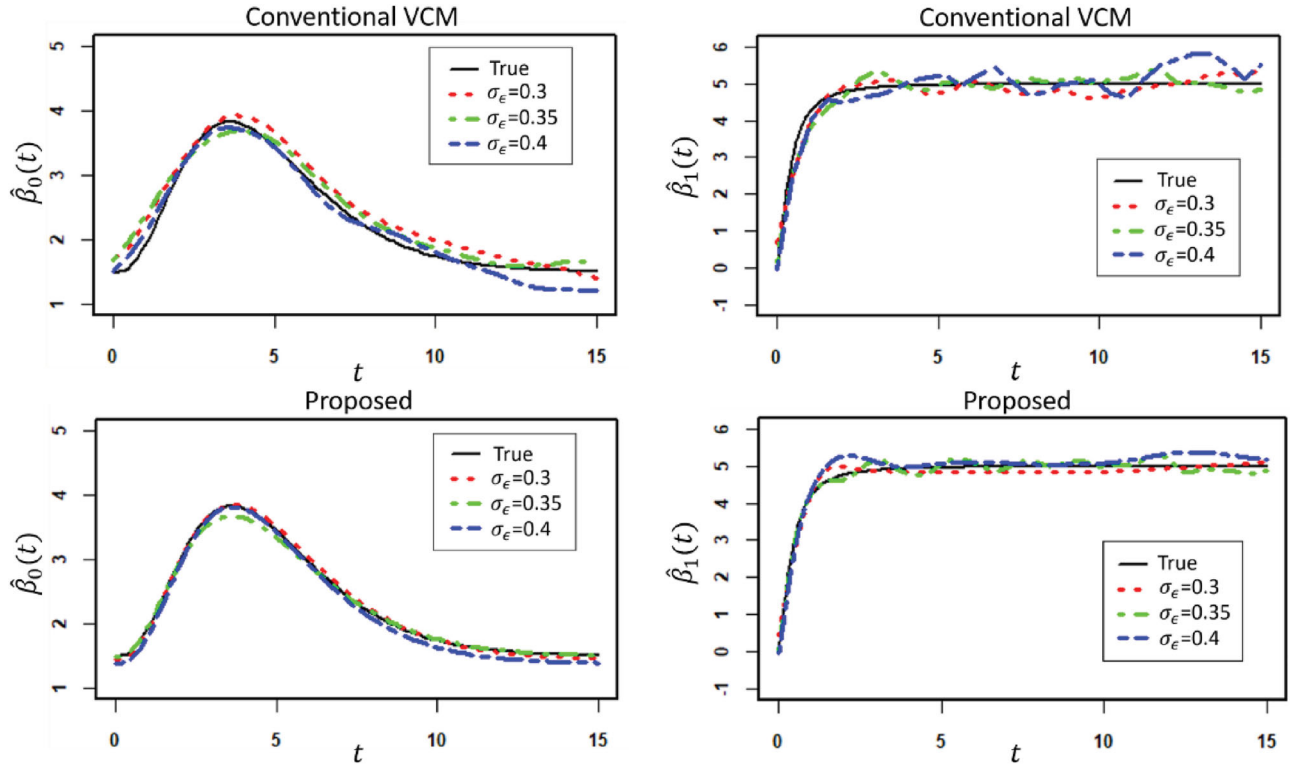

Figure 14. Estimates of $\beta_0(t)$ and $\beta_1(t)$ using the conventional VCM and the proposed model with the dynamic stability constraint under different noise levels ($n = 30$).

and the additional time needed for imposing the dynamic stability constraint is under 10 sec on a 2.20 GHz processor.

Figure 14 shows the estimation results for the two methods under the different noise levels, with the sample size $n = 30$. We first examine the red dashed curves in the plots, which are the estimates of the data shown in Figure 13 (i.e., $\sigma_\epsilon = 0.3$). For the conventional VCM, the estimated $\beta_0(t)$ has distinct deviations from the true curve, and the estimated $\beta_1(t)$ has large fluctuations in the later stage and deviates substantially from the true curve. For the proposed model, the estimated $\beta_0(t)$ is close to the true curve, and the estimated $\beta_1(t)$ exhibits convergence behavior in the later stage and becomes close to the true curve. This validates that the use of the dynamic stability constraint in the estimation of $\beta_1(t)$ can improve the fitting performance and produce interpretable results consistent with expert knowledge.

Regarding the effect of the noise level, the estimation performance of both methods becomes worse when the noise level increases. Overall, the estimates of the proposed model are closer to the true curves in all cases. Figure 15 shows the estimation results under different sample sizes, with the noise level $\sigma_\epsilon = 0.3$. Similarly, the estimation performance of both methods becomes worse when the sample size decreases, and the proposed model performs better in all cases.

7. Discussion

This study proposes a constrained VCM method to model data from time-course experiments in the fabrication of artificial soft tissues. It can accommodate expert knowledge about the baseline material property and the effect of the process parameter on the material property. According to both the case study and the numerical study, the proposed method leads to an estimated model with good interpretability and accurate prediction performance.

There are several directions for future research. First, it will be interesting to investigate how to extend the proposed semiparametric model to the case of multiple covariates. In this case, the dynamic stability constraint will need to be imposed on each smoothing component. The *mgcv* package in R, which implements GCV optimization with respect to multiple smoothing parameters, would probably be useful for this extension. One possibility is to adapt this algorithm to the penalization approach of the dynamic stability constraint, that is, integrate this constraint into the objective function as multiple penalty terms. We plan to conduct future research along this direction.

Second, in the weighted smoothing spline fitting, we update weights based on residuals from the previous iteration. Though $C_{\widehat{\beta}_1}$ decreases as the iterations increase in the case study, this method does not always guarantee such monotonicity. We have considered other ways to update weights, but they do not appear to perform as well as the proposed method in terms of the convergence performance of $\widehat{\beta}_1(t)$. We will continue to explore other methods for updating weights to find one that performs better than the proposed method.

Finally, this study considers a single constraint in the modeling. A more general scenario in practice is that multiple constraints need to be considered simultaneously. For example, a process parameter may affect the product property of interest in a monotonic way, with its effect simultaneously also following a convergence pattern. In such a case, two constraints—monotonicity and stability—need to be incorporated, which is a challenging problem. The problem becomes even more

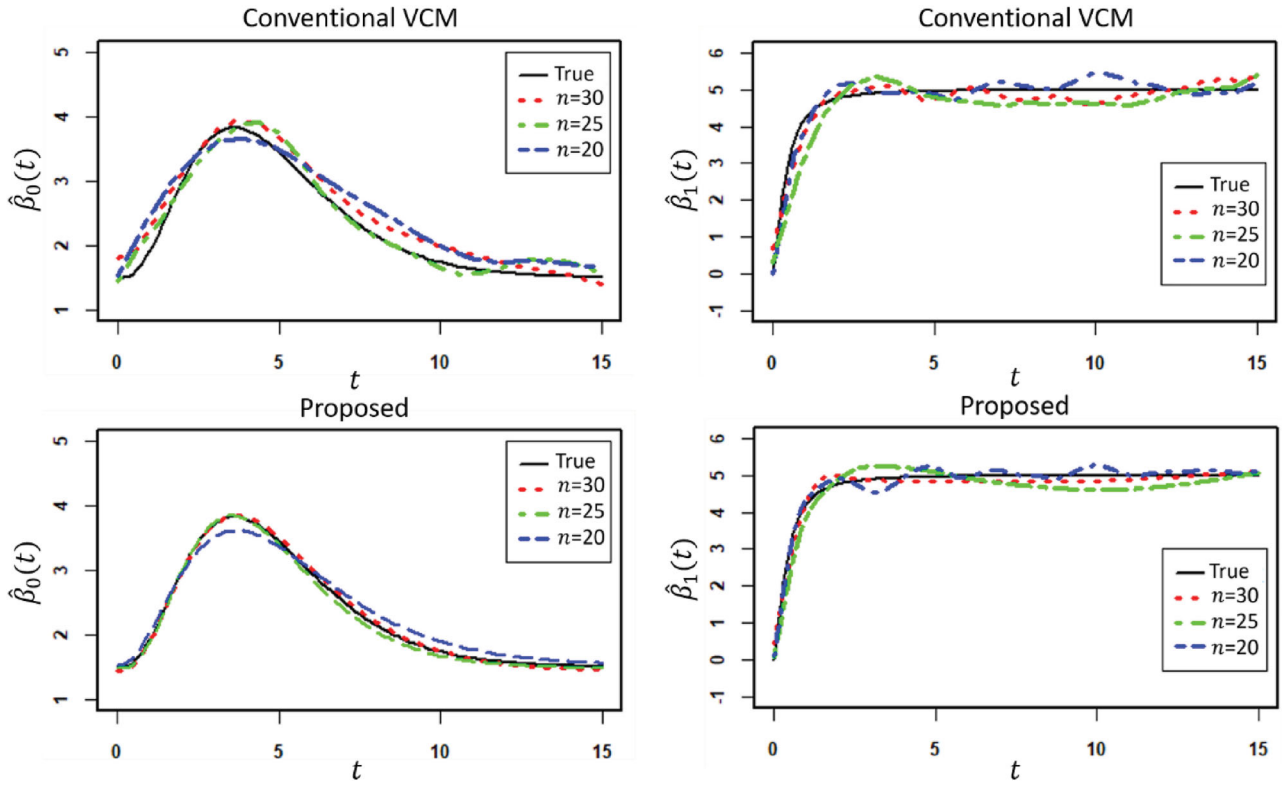

Figure 15. Estimates of $\beta_0(t)$ and $\beta_1(t)$ using the conventional VCM and the proposed model with the dynamic stability constraint under different sample sizes ($\sigma_\epsilon = 0.3$).

complex when multiple process parameters are involved. One can imagine a case where a monotonicity constraint applies to one process parameter while a stability constraint applies to another. We will systematically explore these problems in our future research.

Supplementary Materials

Online supplementary materials for this article include technical proofs, algorithms, and the data and R code used in the case study and the numerical study.

Acknowledgments

The authors sincerely thank the associate editor and two anonymous reviewers for their valuable comments and suggestions that helped improve this article.

Funding

This work is supported by the National Science Foundation under grant CMMI-1634858.

References

Anderssen, R. S., and Bloomfield, P. (1974), "Numerical Differentiation Procedures for Non-Exact Data," *Numerische Mathematik*, 22, 157–182. [5]

Bochynska, A. I., Hannink, G., Grijpma, D. W., and Buma, P. (2016), "Tissue Adhesives for Meniscus Tear Repair: An Overview of Current Advances and Prospects for Future Clinical Solutions," *Journal of Materials Science: Materials in Medicine*, 27, 85. [1]

Coleman, T., and Li, Y. (1996), "An Interior Trust Region Approach for Nonlinear Minimization Subject to Bounds," *SIAM Journal on Optimization*, 6, 418–445. [5]

Craven, P., and Wahba, G. (1978), "Smoothing Noisy Data With Spline Functions: Estimating the Correct Degree of Smoothing by the Method of Generalized Cross-Validation," *Numerische Mathematik*, 31, 377–403. [5]

Davies, P. L., and Meise, M. (2008), "Approximating Data With Weighted Smoothing Splines," *Journal of Nonparametric Statistics*, 20, 207–228. [5,6,7]

Ehrenhofer, A., Elstner, M., and Wallmersperger, T. (2018), "Normalization of Hydrogel Swelling Behavior for Sensoric and Actuatoric Applications," *Sensors and Actuators B: Chemical*, 255, 1343–1353. [8]

Eubank, R. L., Huang, C., Maldonado, Y. M., Wang, N., Wang, S., and Buchanan, R. J. (2004), "Smoothing Spline Estimation in Varying-Coefficient Models," *Journal of the Royal Statistical Society*, Series B, 66, 653–667. [4,5]

Fox, A. J. S., Bedi, A., and Rodeo, S. A. (2012), "The Basic Science of Human Knee Menisci: Structure, Composition, and Function," *Sports Health: A Multidisciplinary Approach*, 4, 340–351. [1]

Hastie, T., and Tibshirani, R. (1993), "Varying-Coefficient Models," *Journal of the Royal Statistical Society*, Series B, 55, 757–796. [2]

He, Y., Xue, G. H., and Fu, J. Z. (2015), "Fabrication of Low Cost Soft Tissue Prostheses With the Desktop 3D Printer," *Scientific Reports*, 4, 6973. [1]

Hsiao, C. (2003), *Analysis of Panel Data*, Cambridge, UK: Cambridge University Press. [3]

Hurvich, C. M., Simonoff, J. S., and Tsai, C.-L. (1998), "Smoothing Parameter Selection in Nonparametric Regression Using an Improved Akaike Information Criterion," *Journal of the Royal Statistical Society*, Series B, 60, 271–293. [5]

Hwangbo, H., Johnson, A. L., and Ding, Y. (2018), "Spline Model for Wake Effect Analysis: Characteristics of a Single Wake and Its Impacts on Wind Turbine Power Generation," *IISE Transactions*, 50, 112–125. [3]

Islam, N. (1995), "Growth Empirics: A Panel Data Approach," *The Quarterly Journal of Economics*, 110, 1127–1170. [3]

Laird, N. M., and Ware, J. H. (1982), "Random-Effects Models for Longitudinal Data," *Biometrics*, 38, 963–974. [3]

Lee, T. C. M. (2003), "Smoothing Parameter Selection for Smoothing Splines: A Simulation Study," *Computational Statistics & Data Analysis*, 42, 139–148. [5]

Lenk, P. J., and Choi, T. (2017), "Bayesian Analysis of Shape-Restricted Functions Using Gaussian Process Priors," *Statistica Sinica*, 27, 43–69. [3]

Lin, L., and Dunson, D. B. (2014), "Bayesian Monotone Regression Using Gaussian Process Projection," *Biometrika*, 101, 303–317. [3]

Maria, L., and Malva, O. (2005), "Contour Smoothing Based on Weighted Smoothing Splines," in *Developments in Spatial Data Handling*, Berlin, Heidelberg: Springer Berlin Heidelberg, pp. 125–136. [5]

Moré, J. J. (1978), "The Levenberg–Marquardt Algorithm: Implementation and Theory," *Numerical Analysis*, 630, 105–116. [5]

Murphy, W., Black, J., and Hastings, G. (eds.) (2016), *Handbook of Biomaterials* (2nd ed.), New York: Springer. [3]

Ortman, J. M., Velkoff, V. A., and Hogan, H. (2014), *An Aging Nation: The Older Population in the United States*, Washington, DC: U.S. Department of Commerce. [1]

Parker, B. R., Hurwitz, S., Spang, J., Creighton, R., and Kamath, G. (2016), "Surgical Trends in the Treatment of Meniscal Tears: Analysis of Data From the American Board of Orthopaedic Surgery Certification Examination Database," *The American Journal of Sports Medicine*, 44, 1717–1723. [1]

Pya, N., and Wood, S. N. (2015), "Shape Constrained Additive Models," *Statistics and Computing*, 25, 543–559. [3]

Qi, L., Sun, Y., and Gilbert, P. B. (2017), "Generalized Semiparametric Varying-Coefficient Model for Longitudinal Data With Applications to Adaptive Treatment Randomizations," *Biometrics*, 73, 441–451. [4]

Rousseeuw, P. (1987), *Robust Regression and Outlier Detection*, Hoboken, NJ: Wiley. [6]

Sadeghi, M., and Hosseinzadeh, H. (2013), "Synthesis and Properties of Collagen-g-Poly(Sodium Acrylate-co-2-Hydroxyethylacrylate) Superabsorbent Hydrogels," *Brazilian Journal of Chemical Engineering*, 30, 379–389. [8]

Slaughter, B. V., Blanchard, A. T., Maass, K. F., and Peppas, N. A. (2015), "Dynamic Swelling Behavior of Interpenetrating Polymer Networks in Response to Temperature and pH," *Journal of Applied Polymer Science*, 132, 42076. [8]

Steiner, S., Jensen, W. A., Grimshaw, S. D., and Espen, B. (2016), "Nonlinear Profile Monitoring for Oven-Temperature Data," *Journal of Quality Technology*, 48, 84–97. [8]

Verbeke, G., Fitzmaurice, G. E., Davidian, M., and Molenberghs, G. (2008), *Longitudinal Data Analysis*, New York: Chapman and Hall/CRC. [3]

Wahba, G. (1985), "A Comparison of GCV and GML for Choosing the Smoothing Parameter in the Generalized Spline Smoothing Problem," *The Annals of Statistics*, 13, 1378–1402. [5]

Wahba, G., and Wold, S. (1975), "A Completely Automatic French Curve: Fitting Spline Functions by Cross Validation," *Communications in Statistics*, 4, 1–17. [5]

Wakefield, J. (2013), *Bayesian and Frequentist Regression Methods*, New York: Springer. [5]

Wang, J., Wei, J., Su, S., Qiu, J., and Wang, S. (2015), "Ion-Linked Double-Network Hydrogel With High Toughness and Stiffness," *Journal of Materials Science*, 50, 5458–5465. [7,9]

Wang, X., and Berger, J. O. (2016), "Estimating Shape Constrained Functions Using Gaussian Processes," *SIAM/ASA Journal on Uncertainty Quantification*, 4, 1–25. [3]

Wei, J., Wang, J., Su, S., Wang, S., Qiu, J., Zhang, Z., Christopher, G., Ning, F., and Cong, W. (2015), "3D Printing of an Extremely Tough Hydrogel," *RSC Advances*, 5, 81324–81329. [1]

Weiss, B., Dakkak, M., Rockl, G., Sukhu, B., Mohr, J., Maru, K., and Eye and Tissue Data Committee (2017), "Development of National System Performance Metrics for Tissue Donation, Production, and Distribution Activity," *Cell and Tissue Banking*, 18, 281–296. [1]

Wood, S. N. (2011), "Fast Stable Restricted Maximum Likelihood and Marginal Likelihood Estimation of Semiparametric Generalized Linear Models," *Journal of the Royal Statistical Society*, Series B, 73, 3–36. [5]

World Health Organization (2011), "Global Health and Aging," NIH Publication No. 11-7737. [1]

Yang, W., Bitetti-Putzer, R., and Karplus, M. (2004), "Free Energy Simulations: Use of Reverse Cumulative Averaging to Determine the Equilibrated and the Time Required for Convergence," *The Journal of Chemical Physics*, 120, 2618–2628. [6]

Zeger, S. L., and Diggle, P. J. (1994), "Semiparametric Models for Longitudinal Data With Application to CD4 Cell Numbers in HIV Seroconverters," *Biometrics*, 50, 689–699. [3]

Zeng, L., Deng, X., and Yang, J. (2016), "Constrained Hierarchical Modeling of Degradation Data in Tissue-engineered Scaffold Fabrication," *IISE Transactions*, 48, 16–33. [3]

Zeng, L., Deng, X., and Yang, J. (2018), "Constrained Gaussian Process With Application in Tissue-Engineering Scaffold Biodegradation," *IISE Transactions*, 50, 431–447. [3]